Effect of heat loss on performance of thin film thermoelectric

A mathematical model

M. Hosseini, S. Mojtaba; Rezaniakolaei, Alireza; Rosendahl, Lasse

Published in:
Materials Research Express

DOI (link to publication from Publisher):
10.1088/2053-1591/aafba1

Publication date:
2019

Document Version
Accepted author manuscript, peer reviewed version

Effect of heat loss on performance of thin film thermoelectric; A mathematical model

To cite this article before publication: Mojtaba Mirhosseini *et al* 2019 *Mater. Res. Express* in press https://doi.org/10.1088/2053-1591/aafba1

Effect of Heat Loss on Performance of Thin Film Thermoelectric; A Mathematical Model

Mojtaba Mirhosseini, Alireza Rezania*, Lasse Rosendahl

Department of Energy Technology, Aalborg University, Pontoppidanstraede 111, 9220 Aalborg East, Denmark

Abstract

To produce a higher electrical power in thin film thermoelectric legs, one way is to conduct the heat flow in-plane parallel to the surface of thin films. One important advantage of using the thermoelectric element in-plane is that, due to high thermal resistance of the thermoelectric leg, there is no need for an efficient heat sink at cold side. A comprehensive mathematical model for analyzing performance of a ZnSb based thermoelectric thin film is proposed based on one dimensional (1D) steady state analysis. Finite element method is employed to solve governing equations, and effects of temperature dependency of thermoelectric material are considered in the model. The modeling study is carried out by a comparison between the ideal case, where there is no heat loss from the thin film, and the case that the heat loss accrues from lateral surfaces of the thin film to the ambient. By taking side surface heat transfer into account for both vertical and horizontal placement of the thin film, two different nonlinear temperature distributions along the thin film length are obtained, and variation of matched power output versus different thermal boundary conditions is shown. The results show that convective heat transfer to the ambient reduces thermoelectric power output, especially at higher temperature difference between the hot and cold sides of the leg. Furthermore, different parameters such as Seebeck coefficient, temperature, generated Seebeck voltage, heat loss, thermoelectric voltage and current at peak power point are evaluated for vertical and horizontal thin film configurations.

Keywords: *Thin Film Thermoelectric Generator (TFTEG); Side Surface Heat Loss; Seebeck Coefficient; Matched Power Output; Finite Element Method (FEM); Zinc Antimonide.*

* Corresponding author: Alireza Rezania. E-mail: alr@et.aau.dk

Nomenclatures

T_h : Hot side temperature	$T_{TEG,c}$: Thin film temperature at cold junction
T_c : Cold side temperature	$\dot{Q}_{TE,i}$: Conduction through the i^{th} element
α : Seebeck coefficient	$R_{t,h}$: Thermal resistance of the hot side
$\dot{Q}_h$: Conductive heat transfer in hot side of thin film	$R_{t,c}$: Thermal resistance of the cold side
$\dot{Q}_c$: Conductive heat transfer in cold side of thin film	$\dot{Q}_{Peltier,i}$: Peltier heat transfer of i^{th} element
$\dot{Q}_{loss,i}$: Heat loss from i^{th} element	$R_{t,TE,i}$: Thermal resistance of i^{th} element
$\dot{Q}_{Joule,i}$: Joule heating of i^{th} element	$R_{e,TE,i}$: Electrical resistance of i^{th} element
$T_{TEG,h}$: Thin film temperature at hot junction	I: Electrical current
Ra_L : Rayleigh number	β: Air expansion coefficient
$\overline{Nu}_L$: Average Nusselt number	T_e: Average temperature of element
Pr : Prandtl number	T_∞ : Ambient temperature
L: Characteristic length	ν : Kinematic viscosity
$\acute{a}$: Thermal diffusivity factor of air	T_i : Temperature of i^{th} node
$T_{f,e,i}$: Air film temperature of i^{th} element	$\overline{Nu}_{L,i}$: Average Nusselt number of i^{th} element (Vertical)
ΔT : Temperature difference between hot and cold junctions of thin film	$\overline{Nu}_{L,top,i}$: Average Nusselt number of i^{th} element (top surface of horizontal thin film)
$k_{f,i}$: Air thermal conductivity near i^{th} element at film temperature	$\overline{Nu}_{L,bottom,i}$: Average Nusselt number of i^{th} element (bottom surface of horizontal thin film)
A : One side lateral area of element	V_{gen} : Generated Seebeck voltage
P : One side perimeter of element	PPP : Peak power point
$\bar{\alpha}$: Average Seebeck coefficient of thin film	$T_{e,i}$: Average temperature of i^{th} element

1. Introduction

Traditionally, in analytical models for design and performance evaluation of thermoelectric generators (TEGs), material properties are assumed constants along the leg length, and average temperature of the cold and hot sides are used for the calculations [1]. Heat loss at the junctions between heat sink and heat source are considered mostly with constant material properties [2-4], while temperature dependent material properties affects profile of the heat flow from the hot side to the cold side of a TEG [5]. Different numerical approaches such as finite element method (FEM) and finite volume method (FVM) have been used to consider temperature dependent material properties for evaluation of TEG modules performance.

Many researchers have conducted their performance analyses and optimization of TE devices based on the generalized thermoelectric energy balance equations. These generalized equations involve the internal irreversibility of Joule heating inside the thermoelectric legs and heat leakage through the thermoelectric elements. However, it is usually assumed that the TEG is thermally isolated from the surroundings except for the heat flows at the cold and hot junctions.

Xiao et al. [6] carried out a detailed modeling and analyzing of a multi-element bulk TEG module. In their investigation, exergy analysis was performed to the irreversible heat transfer process in particular. Shen et al. [7] investigated theoretical modeling of thermoelectric generator performance particularly by considering the effect

of heat transfer from side surfaces. They found that, as the side surface convective heat transfer coefficient decreases, the efficiency increases. However, the matched power output depends on convection rates and thermoelectric materials. Performance of a TEG device, designed to convert engine exhaust heat directly into electricity, was studied under different operating conditions by Zhang [5]. A theoretical model was developed to evaluate different effective factors in order to optimize the electric power from low grade waste heat using TEG technology by Rana et al. [8]. Lee et al. [9] developed a mathematical model for a TEG, based on constitutive equations to analyze temperature dependent performance in terms of efficiency and output power. For thermal losses study, conductive and radiative heat transfer was considered in their finite element model.

Although there are few studies that have investigated performance of thin film thermoelectric modules or elements [10-13], for modelling of heat loss in TEGs, only bulk thermoelectric modules are considered so far. As discussed in previous studies [14, 15], one way to enhance electrical power generation by thin film thermoelectric element is to conduct the heat flow parallel to the length of thin film deposited on an insulating substrate. Since, in thin film TEG with longitudinal direction heat flow, the lateral area is large and, the most suitable operating temperature for zinc antimonide thermoelectric material is mid temperature range (200-400 °C), the heat loss between the element and the surrounding is not negligible. Therefore, in present study, mathematical modelling is carried out to estimate thermoelectric performance of a zinc antimonide based thin film that can be used in flexible TEG for sensor applications. Effects of convective heat transfer from the side surfaces of the element under various operating conditions are investigated by using Finite Element Method (FEM) for both vertical and horizontal configurations of the thin film.

2. Theoretical model

FEM has become an extremely worthy solution technique for coupled problems such as thermal-electric performance analysis in many devices and equipment. Herein, for modeling purpose, two copper strips are considered on both sides of the thin film in modelling instead of electrical interconnections of thin film in a module in reality. The cold side copper strip is exposed to the ambient temperature (25 °C) and the hot side copper strip to fixed temperatures. The heat, $\dot{Q}_h$, flows through the hot side thin copper strip, as the heat source with temperature of T_h, and reaches the hot junction of thin film. Along the leg, a fraction of the heat is converted into electrical power via the Seebeck effect of thermoelectric materials under a certain electrical load. On the other hand, a portion of the imposed thermal energy is transferred to the ambient from side surfaces of thin film by convection. The rest of the heat, $\dot{Q}_c$, passes through the cold junction and the cold side thin copper strip and reaches the temperature of T_c. Both copper strips have a width of 0.01 mm, and the same thickness with the thin film (summation of 350 μm substrate thickness and 600 nm thermoelectric material thickness). The thermal conductivity of the copper strips is assumed 400 W/mK. Figure 1 shows a picture and schematic views of the considered thin film in vertical and horizontal placements including nodes and elements in FEM model.

Figure 2 illustrates the thermal resistance networks and type of heat exchanging mechanisms through the elements and nodes. As shown, a term of $\dot{Q}_{loss}$ should additionally be considered in the analyses since the effect of the heat transfer from the side surface is taken into account. A brief summary of equations explaining the thermal-electric analysis in this problem are mentioned as follows.

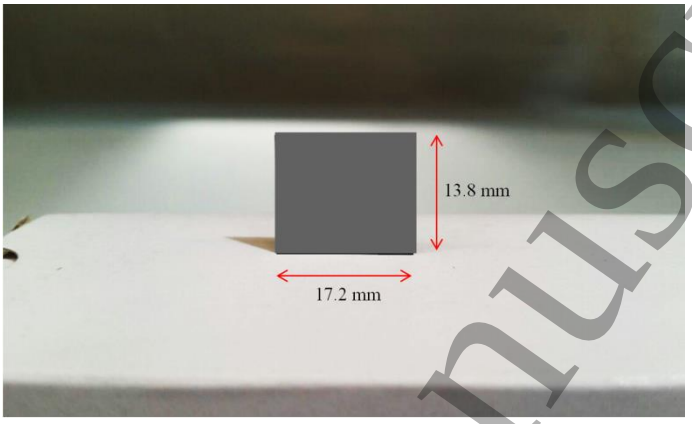

a)

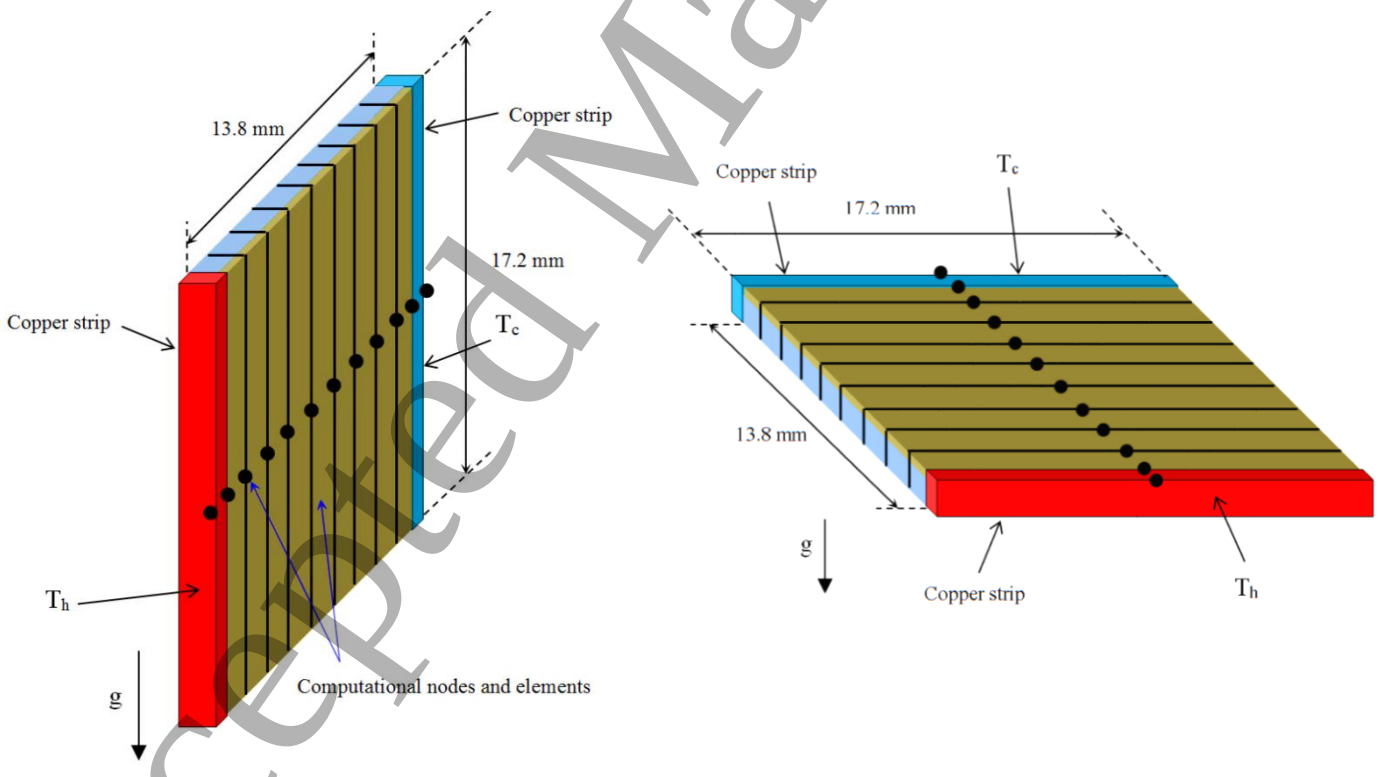

b) c)

Fig. 1: a) Picture of the zinc antimonide thin film specimen; Schematic view of the thin film, nodes and elements, copper strips at hot and cold junctions; b) Vertical placement; c) Horizontal placement

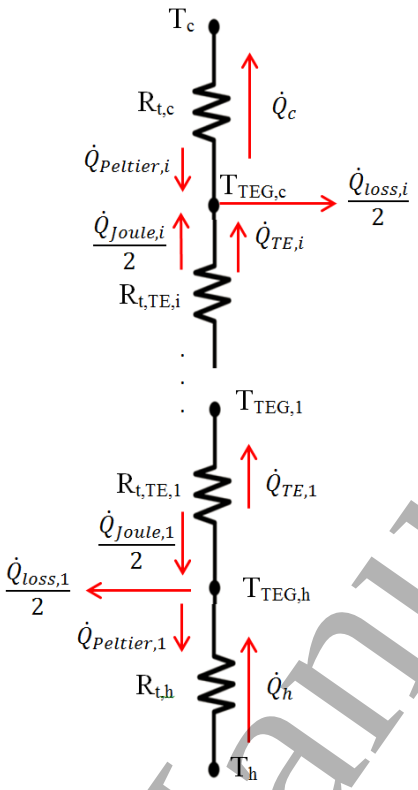

Fig. 2: One dimensional thermal equivalent electrical circuit

The thermal resistance of the hot side is shown by $R_{t,h}$ that can be used for calculating the conductive heat transfer across the copper strip. Moreover, $R_{t,c}$ represents the thermal resistance of the copper strip at the cold side. The model, furthermore, includes effects of the Joule and Peltier heating. Based on the FEM method, length of the thin film is divided into a number of elements. The energy balance for the first and last nodes of the thin film is given by Eqs. (1-10). Temperatures of these nodes are represented by $T_{TEG,h}$ and $T_{TEG,c}$. For the hot junction on the thin film, equations can be written as:

$$\dot{Q}_h - \dot{Q}_{TE,1} - \dot{Q}_{Peltier,1} + \frac{\dot{Q}_{Joule,1}}{2} - \frac{\dot{Q}_{loss,1}}{2} = 0 \quad (1)$$

$$\dot{Q}_h = \frac{T_h - T_{TEG,h}}{R_{t,h}} \quad (2)$$

$$\dot{Q}_{TE,1} = \frac{T_{TEG,h} - T_{TEG,1}}{R_{t,TE,1}} \quad (3)$$

$$\dot{Q}_{Peltier,1} = \alpha\, T_{TEG,h}\, I \quad (4)$$

$$\dot{Q}_{Joule,1} = I^2\, R_{e,TE,1} \quad (5)$$

The Joule heating ($\dot{Q}_{Joule}$) is a volumetric heat generation mechanism, that half of this heat is taken into consideration at the hot and cold junctions of each element. Transferring of the thermal energy between two

junctions of each element by the Peltier effect is shown as $\dot{Q}_{Peltier}$. The Thomson heat effect is neglected in this study, because of its lower contribution in comparison with other thermo-electrical heat transfer mechanism in mid temperature range [16, 17]. For the cold junction of the thin film we have:

$$\dot{Q}_c - \dot{Q}_{TE,i} - \dot{Q}_{Peltier,i} - \frac{\dot{Q}_{Joule,i}}{2} + \frac{\dot{Q}_{loss,i}}{2} = 0 \quad (6)$$

$$\dot{Q}_c = \frac{T_{TEG,c} - T_c}{R_{t,c}} \quad (7)$$

$$\dot{Q}_{TE,i} = \frac{T_{TEG,i-1} - T_{TEG,c}}{R_{t,TE,i}} \quad (8)$$

$$\dot{Q}_{Peltier,i} = \alpha\, T_{TEG,c}\, I \quad (9)$$

$$\dot{Q}_{Joule,i} = I^2\, R_{e,TE,i} \quad (10)$$

For an arbitrary node between the above mentioned nodes, Eq. 11 is used. Fundamental descriptions and preliminary discussion about modelling of TEG modules and energy balance equations have been explained in literature [7, 18].

$$\dot{Q}_{TE,i-3} - \dot{Q}_{TE,i-2} + \dot{Q}_{Peltier,i-3} - \dot{Q}_{Peltier,i-2} + \frac{\dot{Q}_{Joule,i-3}}{2} + \frac{\dot{Q}_{Joule,i-2}}{2} - \frac{\dot{Q}_{loss,i-2}}{2} - \frac{\dot{Q}_{loss,i-3}}{2} = 0 \quad (11)$$

Similar to Eq. (11) can be written for all internal nodes between the hot and cold junctions of the thin film. By making a system of equations for the studied nodes using the FEM and solving it and defined boundary conditions, the unknown temperatures of the nodes can be determined. The cold side copper strip is exposed to the ambient temperature at 25 °C, while the copper strip at the hot side is exposed to fixed temperatures, 150, 200, 250, 300 and 350 °C. The term of $\dot{Q}_{loss,i-2}$ shows the heat loss from element (i-2)th and $\dot{Q}_{loss,i-3}$ is the heat loss from element (i-3)th. Therefore, the total convective heat loss from (i-3) th node becomes equal to summation of half of the convective heat loss from element (i-2)th and half of the convective heat loss from element (i-3)th that is transferred to the surrounding (see Fig. 2). The thermal conductivity, electrical resistivity and Seebeck coefficient of each element of the ZnSb thin film are calculated as functions of temperature obtained experimentally in another study [19]. The curve fitting allows estimating the properties from ambient temperature to an upper practical temperature, which is around 400 °C for ZnSb based materials used as p-type material. To include effect of free convection of the vertical thin film to the ambient, an empirical correlation for average Nusselt number (Nu) can be applied for laminar flows, where Rayleigh number (Ra) is less than 10^9 [20].

$$\overline{Nu}_L = 0.68 + \frac{0.67\, Ra_L^{(1/4)}}{\left[1 + \left(0.492/Pr\right)^{(9/16)}\right]^{(4/9)}} \quad (12)$$

$$Ra_L = \frac{g\beta(T_e - T_\infty)L^3}{\nu\acute{\alpha}} \quad (13)$$

where *Pr* is the Prandtl number, and *L* is characteristic length defined based on the external flow geometry. In this study, *L* is height of the vertical thin film (17.2 mm). The parameter β is expansion coefficient of air. Parameter T_e represents the average temperature of each element that is related to two adjacent nodes of that element. In Eq. (13), T_∞ is the ambient temperature equal to 25 °C in this study. The parameters ν and ά are kinematic viscosity and thermal diffusivity factor of air, respectively. Air properties in the equations are obtained at film temperature [20]:

$$T_{f,e,i} = \frac{\left(\frac{T_i + T_{i-1}}{2}\right) + T_\infty}{2} \quad (14)$$

where T_i and T_{i-1}, are temperatures on thin film at ith and (i-1)th nodes. Furthermore, $T_{f,e,i}$ implies the air film temperature of the ith element. It is worthy to note that, Eq. (12) calculates Nu for one side of the vertical element. Therefore, for two lateral sides of the vertical thin film, effect of the Nu on both sides of the element must be considered for calculation of the heat loss as follows:

$$\dot{Q}_{loss,i} = \left(\frac{2\overline{Nu}_{L,i} k_{f,i}}{L}\right) A(T_{e,i} - T_\infty) \quad (15)$$

where $\overline{Nu}_{L,i}$ is the average Nusselt number of ith element, $k_{f,i}$ is thermal conductivity of air near the ith element at film temperature, and *A* is the lateral area of one side of the element. Moreover, for calculating heat loss to the ambient in the horizontal placement due to free convection, empirical correlations can be represented for average Nusselt number (Nu) at top and bottom surface of the horizontal plate [20]:

$$\overline{Nu}_{L,top} = 0.54\, Ra_L{}^{1/4} \qquad (10^4 \le Ra_L \le 10^7) \quad (16)$$

$$\overline{Nu}_{L,top} = 0.15\, Ra_L{}^{1/3} \qquad (10^7 \le Ra_L \le 10^{11}) \quad (17)$$

$$\overline{Nu}_{L,bottom} = 0.27\, Ra_L{}^{1/4} \qquad (10^5 \le Ra_L \le 10^{10}) \quad (18)$$

In the horizontal case, *L* is defined as *A/P*, so that *A* is one side lateral area and *P* is perimeter of the rectangular element on thin film. Therefore, the heat loss from the ith element in horizontal placement is obtained by:

$$\dot{Q}_{loss,i} = \left(\frac{(\overline{Nu}_{L,top,i} + \overline{Nu}_{L,bottom,i}) k_{f,i}}{L}\right) A(T_{e,i} - T_\infty) \quad (19)$$

To solve the algebraic equations for analyzing performance of the thin film, a computer program in MATLAB software was developed and compiled. Firstly, the number of elements and initial temperatures of all nodes along the leg are assumed. Then, according to the initial temperature distribution, physical properties of each

element are obtained. By solving all the thermal-electrical equations simultaneously, temperature distribution along the leg was achieved. When the absolute temperature difference lower than 10^{-5} between two tandem iterations in each node is satisfied, the iteration stops.

3. Results and discussions

3.1. Discretization independence study

For finding solution with acceptable accuracy and to check dependency of the results to the mesh, the problem is considered over the elements while it is divided into one, four and nine elements. In this study, density of the mesh is high enough and, consequently, the temperature difference between two nodes on each element is small enough to ensure the power generation by the thin film is not influenced if the number of elements increases further. Seebeck coefficient of a homogeneous thermoelectric material only depends on temperature. Therefore, according to temperature distribution along the thin film, the Seebeck coefficient has its own individual distribution. It is worthy to note that, the results in this paper are represented based on calculations at matched power output or peak power point (PPP). The matched power output is obtained when the consumptive electrical load is equal to the TEG electrical resistance [10-12, 21, and 22].

Figure 3 shows the average Seebeck coefficient by adopting different temperatures at the hot side. As number of the nodes increases, accuracy of the results enhances, however the rate of improvement of the accuracy clearly reduces from the 5-node model to the 10-node model. Therefore, the solution can be considered relatively independent to node number more than 5. Furthermore, there is not noticeable difference between the results of the 5-node and 10-node models either with or without side surface heat loss. Heat loss effect causes reduction of the average Seebeck coefficients; however this reduction is more significant for the vertical placement of thin film. The 2-node model cannot predict effect of heat loss from the side surfaces because the Seebeck coefficient of the thin film is only related to the temperature of the junctions of two sides. By increasing the hot side temperature, the average Seebeck coefficient increases continuously for all the studied cases, except for the 5-node and 10-node models at zero heat loss cases, which have maximum values when the hot side temperature is 300 ^{o}C. At 300 ^{o}C, temperatures of the most elements along the thin film in these cases are close to the temperature which corresponds to the maximum Seebeck coefficient. At temperatures higher than 300 ^{o}C, bipolar transport effect [11, 12] appears and the Seebeck coefficient of some elements reduces; so that the average Seebeck coefficient reduces. Although, by considering the heat loss for the both vertical and horizontal placements, the number of elements that have temperatures in the range of maximum Seebeck coefficient reduces. Therefore, in the studied range of temperature, average Seebeck coefficient increases monotonically and the maximum value of average coefficient is only observed for cases without heat loss consideration. In absence of the heat loss, performance of the vertical and horizontal placements of the thin film are the same.

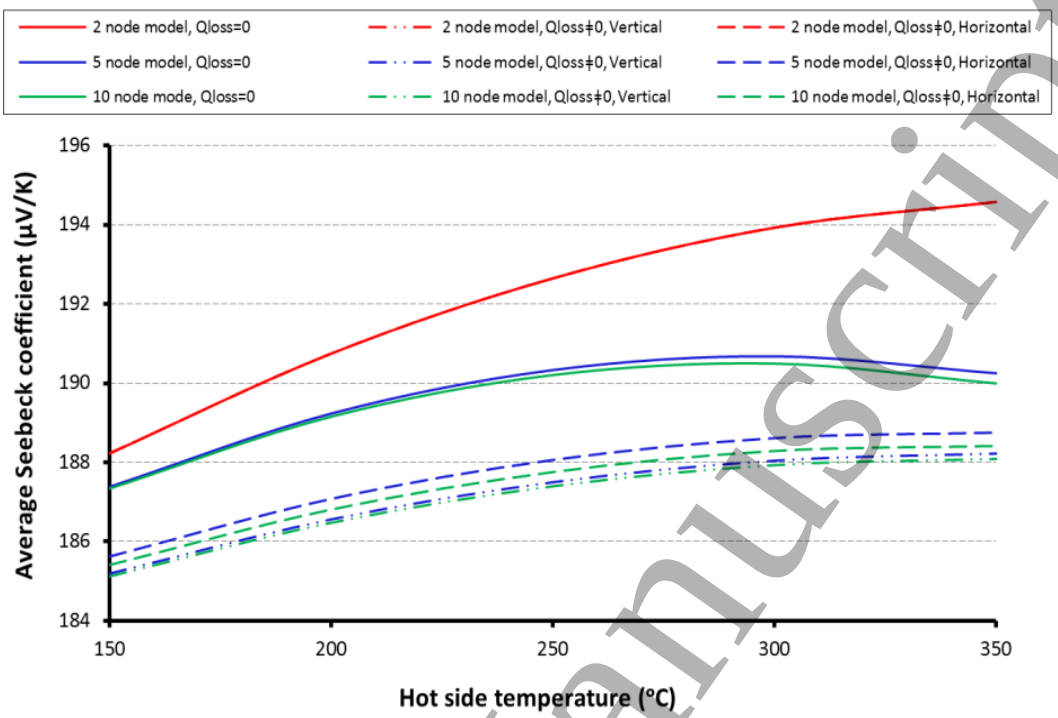

Fig. 3: average Seebeck coefficient versus different hot side temperatures at PPP

Figure 4 shows calculated total heat loss for different hot side temperatures. Comparing the results shows that 5-node model has good accuracy, whereas the 10-node model is more precise. The 2-node model is not capable to estimate the middle nodes temperatures and is not sensitive to the heat loss consideration. For the horizontal configuration, the total heat loss obtained by the 2, 5 and 10-node models are closer to each other than the results of the vertical placement case. In all studied models, the heat loss increases by rising the hot side temperature with an incremental slope, however a further slope is observed for the 2-node model. Due to highest precision, the 10-node model is chosen for further evaluation of the thin film performance.

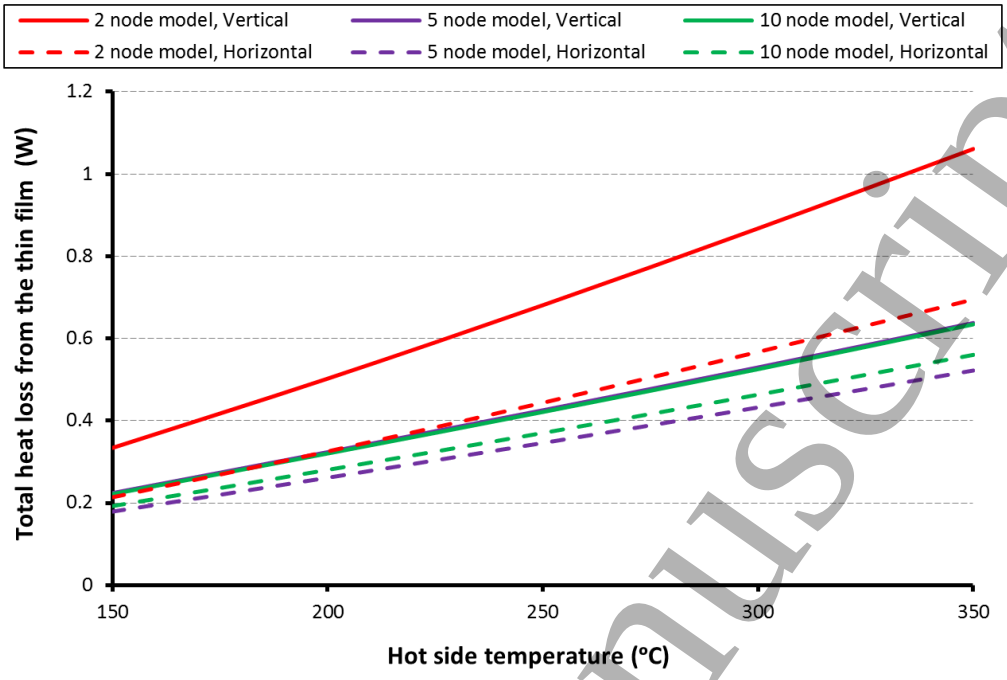

Fig. 4: Total heat loss from the thin film versus hot side temperature at PPP

3.2. Local temperature and heat loss distribution

Figure 5 indicates that the temperature distribution along the thin film is approximately linear and independent to the placement direction when there is no heat loss from the elements. The nonlinear trends are observed by considering the convective heat loss from the side surface for both vertical and horizontal thin film placements. The gradient of temperature corresponding to the heat loss effect is large near the hot junction of thin film. In vertical case with the heat loss, the temperature drop along the thin film is more than the horizontal case due to higher heat transfer coefficient around the vertical thin film for all studied operating conditions.

The local heat loss can be obtained for different cases (Fig. 6). The local heat losses increase as the hot junction temperature enhances. The heat loss distribution depends on the temperature distributions along the thin film, and the heat loss in vertical placement is higher than the horizontal thin film. Free convection occurs due to density variation of the associated flow. The hot air rises up and cold air takes its place in any free convection heat transfer. In case of vertical plate, more contact surface exists for flowing air in comparison with the horizontal plate. Therefore, more contact causes more heat transfer rate, and it gets higher heat transfer coefficient value for vertical plates than horizontal plates [20].

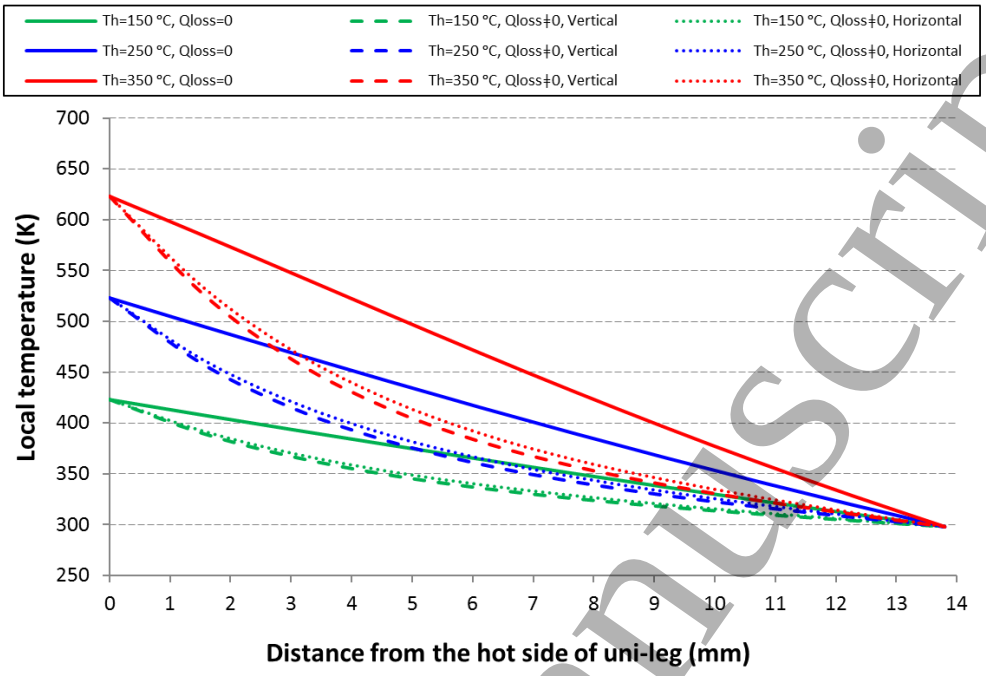

Fig.5: Temperature distribution along the thin film at PPP

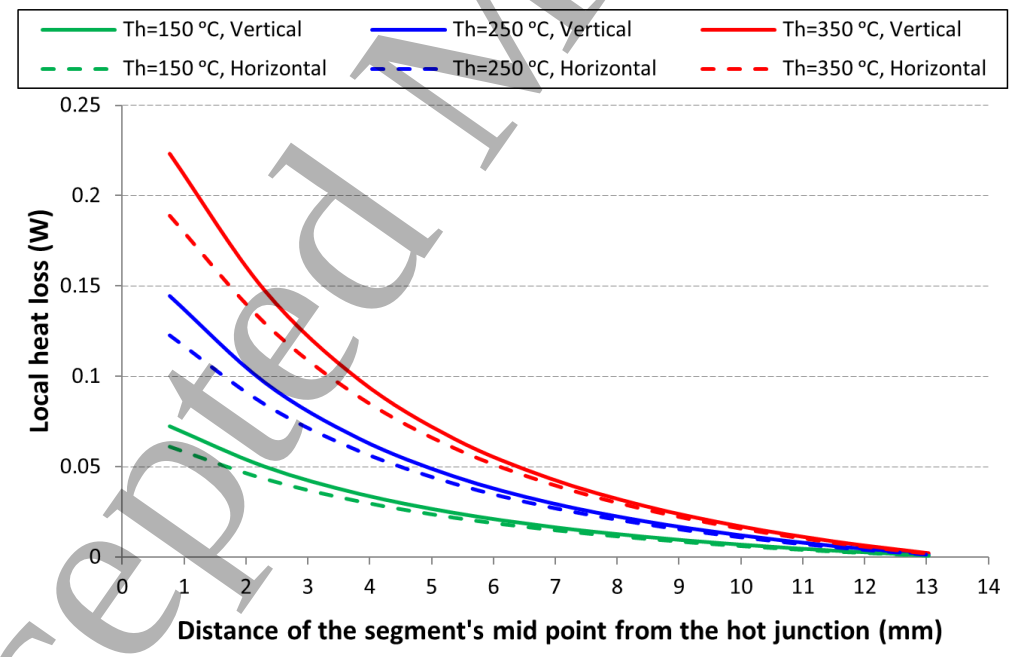

Fig. 6: Local heat loss for different hot side temperatures at PPP

3.3. Seebeck coefficient and Seebeck voltage distribution

The Seebeck coefficient is function of temperature. Figure 7 depicts the Seebeck coefficient in different positions along the thin film. By increasing the hot side temperature, a maximum value appears in Seebeck coefficient distribution shifting toward the cold junction. When the heat loss is considered, the local Seebeck coefficient severely reduces in most of positions compared to the same temperature case with no heat loss. Results show that the highest values of Seebeck coefficient occur for the nodes close to the hot side when the heat loss is taken into account. It is due to the relation between local temperature distribution (see Fig .5) and Seebeck coefficient (see Fig. 7). The values of Seebeck coefficient and particularly temperature gradient approximately in the last 30 % of leg length are small, so that these elements only produce small power rather than others. Furthermore, heat loss from this region is low due to the lower temperature difference with ambient temperature. Similar to the trend of Fig. 5, Seebeck values of the vertical thin film placement are less than the horizontal one.

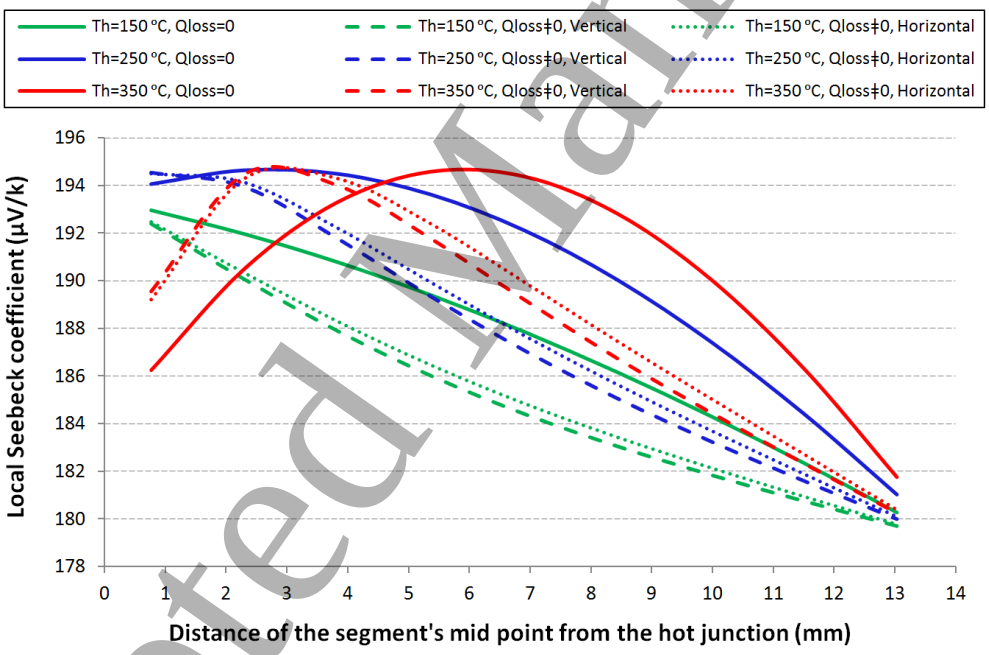

Fig. 7: Local Seebeck coefficient along the thin film at PPP

Local Seebeck voltage (V_{gen}) is shown in Fig. 8 for different hot side temperatures. It is defined as multiplication of local Seebeck coefficient and local temperature gradient along the thin film. In cases without the heat loss, the change in distribution is smooth and without sharp trend, however by considering effect of the heat loss, trend of the Seebeck voltage distribution changes with a sharp reduction from the hot junction to the cold junction as the local temperature reduces. Also, up to 28% of the leg length from the hot junction, the vertical placement of thin film has higher Seebeck voltage than the horizontal arrangement, while in the rest of the thin film length, the Seebeck voltage of the horizontal case becomes higher than the vertical configuration.

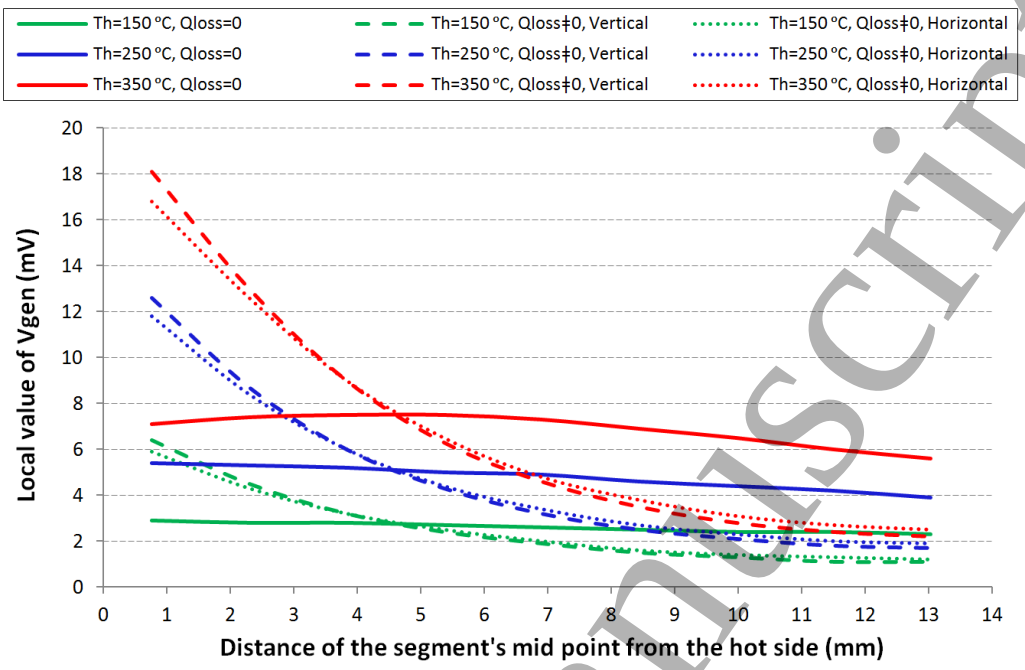

Fig. 8: Local Seebeck voltage along the thin film at PPP

3.4. Electrical resistance and I-V curve

The electrical resistance of each element along the thin film is a function of the local temperature; hence the total electrical resistance is influenced by the thermal boundary conditions and temperature distribution [14]. As illustrated in Fig. 9, by increasing the hot side temperature the electrical resistance reduces. In particular, the slope of reduction is more for the case without heat loss due to higher temperature distribution along the isolated thin film that causes more reduction in local and total electrical resistance. The electrical resistance for vertical placement with heat loss consideration is higher because of its lower temperature.

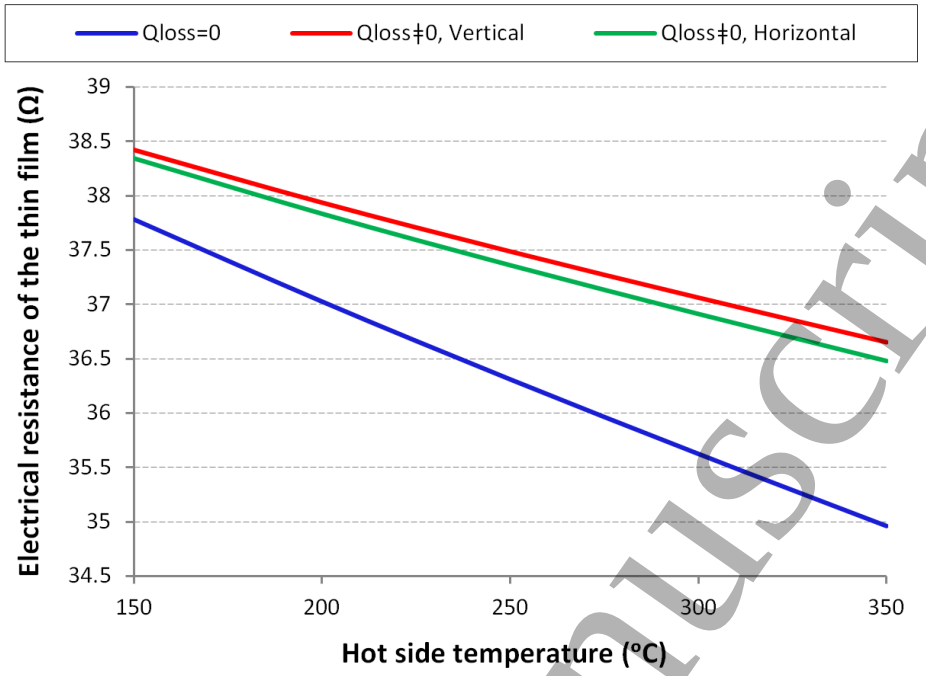

Fig. 9: Total electrical resistance at different hot side temperature

Summation of local Seebeck voltage along the thin film gives the total Seebeck voltage. Total thermoelectric voltage is half of the total Seebeck voltage at peak power point [23] as depicted versus the electrical current in Fig 10. In a fixed hot side temperature, although the total voltage is not influenced by the heat loss, the electrical currents changes significantly by including the heat loss effect. For example, corresponded to each hot side temperature, almost a constant voltage occurs for different thin film configurations, while the current reaches its lowest value in vertical arrangement. However, the current is not much sensitive to vertical or horizontal placement. The letters V and H in the figure legend show the data corresponding to cases with heat loss for vertical and horizontal placements, respectively and Q=0 for the case without heat loss. They have been shown from left to right in the figure legend as V-H-Q=0, as indicated along each line. For higher hot side temperature, difference between the current values of the vertical and horizontal thin film configuration is higher.

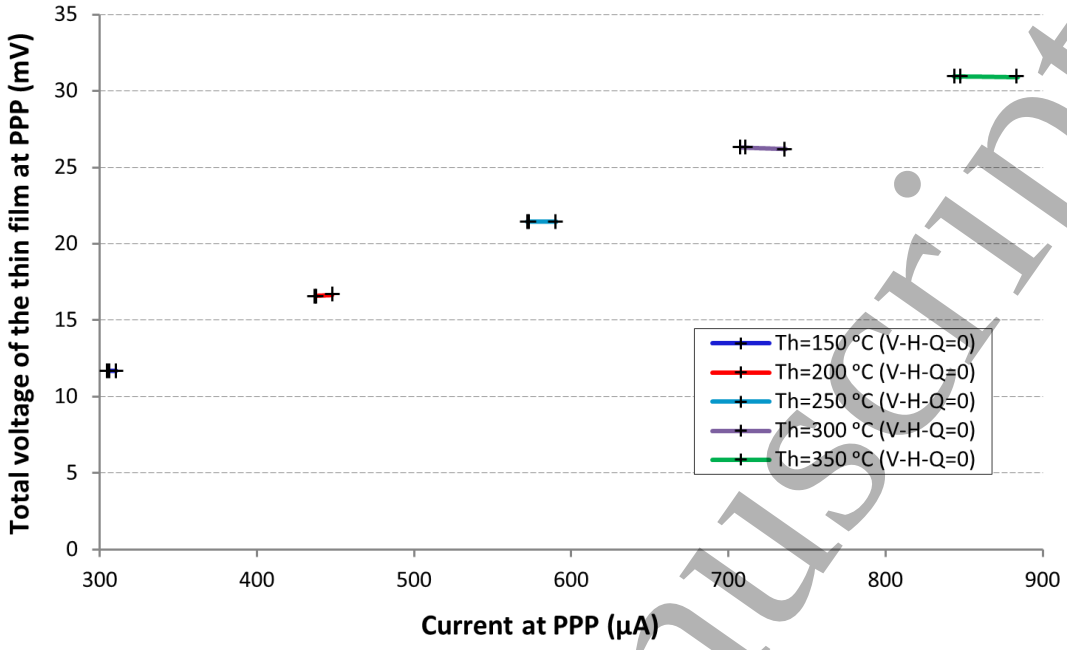

Fig. 10: Thin film total voltage (V_{TEG}) versus electrical current at PPP

3.5. Matched power output

The matched power output is defined as a power generated by the TEG when an external electrical load resistance equal to total electrical resistance (R) of the thermoelectric device is imposed to the electrical circuit. The power generation by the thin film and generally thermoelectric devices can be underestimated or overestimated depending on the operating conditions, test facilities, and thermoelectric materials. The thin film matched power is obtained in each operating conditions as mentioned in the modeling part. Using an analytical relation as $P_{matched}=(\bar{\alpha}^2 \Delta T^2)/4R$ [1, 23], that can be used in absence of heat loss shows a good agreement between the analytical relation and the results from the FEM model.

In Table 1, results of matched power output obtained by 10-node FEM model are compared with the results calculated by the above-mentioned analytical relation in absence and presence of heat loss for both vertical and horizontal arrangements. The FEM model estimates the matched power values higher than the analytical results, because of simplification in the analytical relation. Moreover, the results of FEM model show the heat loss generally reduces the matched power. At 350 ^{o}C the percentage of difference between the matched powers of cases with and without heat loss consideration is 4.5 % and 4.07 %, respectively for vertical and horizontal placement. A comparison between the matched power outputs in vertical and horizontal placements in presence of heat loss indicates that the horizontal thin film can generate more power than the vertical.

Table1: Matched power output of the thin film

Hot side temperature (°C)	Matched power output (μW)			
	$P_{matched} = \frac{(\bar{\alpha}^2 \Delta T^2)}{4R}$	10-node model (FEM)		
		Q_{loss}=0	Q_{loss}≠0 (Vertical)	Q_{loss}≠0 (Horizontal)
150	3.27	3.64	3.58	3.58
200	6.63	7.42	7.25	7.27
250	11.4	12.66	12.27	12.31
300	17.4	19.32	18.59	18.66
350	24.8	27.33	26.10	26.22

The results of this study are compared with previous experimental works [10-12]. The experimental studies were carried out on a zinc antimonide thin film specimen with the same effective length, width, thermoelectric material and thickness of the substrate. Table 2 shows voltages generation in the thin film at hot side temperatures of 200 to 350 °C and under optimal electrical load which produce maximum power. The results show that difference between the two data series is ≤ 20 %, which shows a good agreement between the mathematical modelling and the experimental data. The error is due to trade-off between unavoidable effect of contact resistance and extra length of the specimen in the experimental studies. As reported in the experimental studies, a fraction of the specimen length on each side of the specimen, namely 3 mm, was covered by the hot side block and cold side clamp to hold the sample. This extra effective length was not taken into account in the mathematical modelling. A fraction of the generated thermoelectric voltage is due to the thermoelectric materials in these regions.

Table 2: Comparison of thermoelectric voltages (V_{TEG}) at peak power point (PPP)

Hot side temperature of the specimen (°C)	V_{TEG} (mV) at PPP, Q_{loss}≠0, Experiments, vertical [10, 12]	V_{TEG} (mV) at PPP, Q_{loss}≠0, FEM model (10-node), vertical
200	19.6	16.6
250	26.2	21.5
300	33.0	26.3
350	37.9	31.0

4. Conclusions

There are several researches in literature about theoretical performance modeling of bulk thermoelectric materials and modules; however there is still lack of knowledge about in-plane arrangement of thin film performance modelling with/without considering side surface heat loss. In this study, a FEM model was used to

analyze performance of a ZnSb thin film. In longitudinal direction application of thin films, because of big lateral area versus the thin film cross sectional area, side surface heat loss can play a significant role in power generation and performance. The results showed that by considering the heat loss, the matched power output reduces due to reduction of the Seebeck coefficient and temperature gradient and due to enhancement of the electrical resistance in most locations along the leg. The horizontal placement can produce more power than the vertical thin film if the heat loss is taken into account. The results show that the thin film generates maximum power density of 191.92, 183.29, and 184.11 mW/cm^3 (power per unit volume of the thermoelectric material layer) corresponding to the hot side temperature of 350 ^oC, for the cases without the heat loss and with heat loss in the vertical and horizontal placements, respectively. It is found that, electrical current is more sensitive to the heat loss consideration in comparison with the thermoelectric voltage at peak power output.

Acknowledgment

This work was carried out within the framework of the Center for Thermoelectric Energy Conversion (CTEC), and funded in part by the Danish Council for Strategic Research, Programme Commission on Energy and Environment, under Grant No. 1305-00002B.

References

[1] Rowe, D. M., Min, G., Design theory of thermoelectric modules for electrical power generation, IEE Proceedings - Science, Measurement and Technology, 143 (1996) 351-6.

[2] Rezania A., Rosendahl, L. A., New configurations of micro plate-fin heat sink to reduce coolant pumping power. Journal of Electronic Materials, 41 (2012) 1298-1304.

[3] Rezania, A., Rosendahl, L., A comparison of micro-structured flat-plate and cross-cut heat sinks for thermoelectric generation application. Energy Conversion and Management, 101 (2015) 730-737.

[4] Rezania, A., Rosendahl, L. A., Evaluating thermoelectric power generation device performance using a rectangular microchannel heat sink, Journal of Electronic Materials, 40 (2011) 481–488.

[5] Zhang, T., New thinking on modeling of thermoelectric devices, Applied Energy, 168 (2016) 65–74.

[6] Xiao, H., Gou, X. L., Yang, S., Detailed modeling and irreversible transfer process analysis of a multi-element thermoelectric generator system, Journal of Electronic Materials, 40 (2011) 1195-1201.

[7] Shen, Z. G., Wu, S. Y., Xiao, L., Yin, G., Theoretical modeling of thermoelectric generator with particular emphasis on the effect of side surface heat transfer, Energy 95 (2016) 367-379.

[8] Rana, S., Orr, B., Iqbal, A., Ding, L. C., Akbarzadeh, A., Date, A., Modelling and optimization of low-temperature waste heat thermoelectric generator system, Energy Procedia, 110 (2017) 196-201.

[9] Lee, H., Sharp, J., Stokes, D., Pearson, M., Priya, S., Modeling and analysis of the effect of thermal losses on thermoelectric generator performance using effective properties, Applied Energy, 211 (2018) 987–996.

[10] Mirhosseini, M., Rezania, A., Blichfeld, A. B., Iversen, B. B., Rosendahl, L. A., Experimental investigation of zinc antimonide thin film thermoelectric element over wide range of operating conditions, Physica Status Solidi A, (2017) 00 1700301.

[11] Mirhosseini, M., Rezania, A., Rosendahl, L., Iversen, B. B., Effect of thermal cycling on zinc antimonide thin film thermoelectric characteristics, Energy Procedia, 142 (2017) 519–524.

[12] Mirhosseini, M., Rezania, A., Iversen, B., Rosendahl, L., Energy harvesting from a thermoelectric zinc antimonide thin film under steady and unsteady operating conditions, Materials, 11 (2018), 2365, 1-21.

[13] Fan, P., Zheng, Z. H., Li, Y. Z., Lin, Q. Y., Luo, J. T., Liang, G. X., Cai, X. M., Zhang, D. P., Ye, F., Low-cost flexible thin film thermoelectric generator on zinc based thermoelectric materials, Applied Physics Letters, 106 (2015) 073901-1-4.

[14] Yu, X., Liu, Y., Li, T., Zhou, H., Gao, X., Feng, F., Wang, Y., Thin-film-based thermoelectric energy generator device with a card structure, SENSORS conference, 2012 IEEE, Taipei, Taiwan, DOI: 10.1109/ICSENS.2012.6411445.

[15] Fan, P., Zheng, Z. H., Cai, Z. K., Chen, T. B., Liu, P. J., Cai, X. M., Zhang, D. P., Liang, G. X., Luo, J. T., The high performance of a thin film thermoelectric generator with heat flow running parallel to film surface, Applied Physics Letters, 102 (2013) 033904-1-3.

[16] Rezania, A., Sera, D., Rosendahl, L. A., Coupled thermal model of photovoltaic-thermoelectric hybrid panel for sample cities in Europe, Renewable Energy, 99 (2016) 127-135

[17] Mirhosseini, M., Rezania, A., Rosendahl, L., Harvesting waste heat from cement kiln shell by thermoelectric system, Energy, 168 (2019) 358-369.

[18] Dunham, M. T., Barako, M. T., LeBlanc, S., Asheghi, M., Chen, B., Goodson, K. E., Power density optimization for micro thermoelectric generators, Energy, 93 (2015) 2006-2017.

[19] Sun, Y., Christensen, M., Johnsen, S., Nong, N. V., Ma, Y., Sillassen, M., Zhang, E., Palmqvist, A. E. C., Bøttiger, J., Iversen, B. B., Low-cost high-performance zinc antimonide thin films for thermoelectric applications, Advanced Materials, 2012; 24:1693-1696.

[20] Incropera, F.P., Dewitt, D.P., Bergman, T.L., Lavine, A.S. *Fundamentals of Heat and Mass Transfer*, 6th ed.; John Wiley & Sons, USA, 2007; ISBN-13: 9780471457282.

[21] Sundarraj, P., Taylor, R. A., Banerjee, D., Maity, D., Roy, S. S., Experimental and theoretical analysis of a hybrid solar thermoelectric generator with forced convection cooling, Journal of Physics D: Applied Physics, 50 (2017) 015501-1-11.

[22] Priyadarshi, P., Sharma, A., Mukherjee, S., Muralidharan, B., Superlattice design for optimal thermoelectric generator performance, Journal of Physics D: Applied Physics, 51 (2018) 185301-1-7.

[23] Rezania, A., *Integration of Heat Exchangers with Thermoelectric Modules*, *Thermoelectric Energy Conversion: Basic Concepts and Device Applications*, John Wiley & Sons, 2017. ISBN: 978-3-527-34071-2.